

Nuclear/Circumnuclear Starbursts and Active Galactic Nuclei Mass Accretion in Seyfert Galaxies

Yasuyuki Watabe^{1,2,*}, Nozomu Kawakatu³ and Masatoshi Imanishi³

¹*Center for Computational Sciences, University of Tsukuba, Ten-nodai, 1-1-1 Tsukuba, Ibaraki 305-8577, Japan; watabe@ccs.tsukuba.ac.jp*

²*INAF-Osservatorio Astrofisico di Arcetri, Largo Enrico Fermi 5, 50125 Firenze, Italy*

³*National Astronomical Observatory of Japan, 2-21-1 Osawa, Mitaka, Tokyo 181-8588, Japan*

ABSTRACT

We investigated the correlation between nuclear/circumnuclear starbursts around the active galactic nuclei (AGNs) and the AGN activities for 43 Seyfert galaxies in the CfA and 12 μm samples. We found that circumnuclear starburst luminosity as well as nuclear starburst luminosity are positively correlated with AGN luminosity. Moreover, nuclear starburst luminosity is more strongly correlated with the AGN luminosity normalized with AGN Eddington luminosity than is circumnuclear starburst luminosity. This implies that starbursts nearer the AGN could have a greater effect on AGN mass accretion. We also discuss these results from the viewpoint of the radiation effects from starbursts and sequential starbursts.

Subject headings: galaxies: active — galaxies: nuclei — galaxies: Seyfert — galaxies: starburst — infrared: galaxies

1. INTRODUCTION

Since the discovery of active galactic nuclei (AGNs) the physical mechanism of AGN fueling remains unresolved. Various fueling mechanisms have been considered thus far, for example, tidal torque driven by major/minor galaxy merger (Hernquist 1989; Barnes & Hernquist 1991; Mihos & Hernquist 1996; Taniguchi 1999; Saitoh & Wada 2004), tidal torque from nonaxisymmetric gravitational potential due to a stellar bar (Noguchi 1988; Shlosman et al.

*Research Fellow of the Japan Society for the Promotion of Science (JSPS).

1990; Barnes & Hernquist 1992; Knapen et al. 1995; Benedict et al. 1996; Fukuda et al. 2000), shock or turbulence in the interstellar medium (Fukuda et al. 1998; Montenegro et al. 1999; Wada & Norman 1999, 2001; Maciejewski et al. 2002; Wada et al. 2002; Onodera et al. 2004), and radiation drag from a starburst (Umemura et al. 1997; Fukue et al. 1997; Umemura et al. 1998; Ohsuga et al. 1999).

Numerous observations have gradually clarified circumnuclear starburst events (several hundreds of parsecs to a few kiloparsecs from the center) around AGNs. These starbursts often exhibit patchy and ringlike structures (Pogge 1989; Wilson et al. 1991; Forbes et al. 1994; Marconi et al. 1994; Mauder et al. 1994; Buta et al. 1995; Barth et al. 1995; Leitherer et al. 1996; Maoz et al. 1996; Storchi-Bergmann et al. 1996; Elmouttie et al. 1998; Knapen et al. 2002; Knapen 2005). In addition, hidden nuclear starbursts (within a few hundred parsecs from the center) are found both in Seyfert 1 and 2 galaxies (Imanishi 2002, 2003; Rodríguez-Ardila & Viegas 2003) and the nuclear starburst luminosity is positively correlated with the AGN power (Imanishi & Wada 2004).

These starburst events could strongly influence the structure and the dynamics of gas through the energy input of multiple supernova explosions (Shapiro & Field 1976; Tomisaka & Ikeuchi 1986; Norman & Ikeuchi 1989; Wada & Norman 2002) and the effects of strong radiation (Umemura et al. 1997, 1998; Ohsuga & Umemura 1999, 2001; Kawakatu & Umemura 2002; Watabe & Umemura 2005; Thompson et al. 2005). Especially, for the AGN mass accretion, Wada & Norman (2002) shows the possibility of AGN fueling from the effect of the chaotic disturbance by the nuclear starburst using three-dimensional hydrodynamic simulation. Moreover, Umemura et al. (1997, 1998) have shown that the radiation effects of circumnuclear starburst could cause AGN fueling.

These theoretical and observational results suggest that some connections exist between the nuclear/circumnuclear starburst and AGN activity. Although a relationship between the nuclear starburst and the AGN has been reported (Imanishi & Wada 2004; Davies et al. 2007), this remains uncertain regarding the circumnuclear starburst. Moreover, it is not clear whether a specific relationship exists between AGN mass accretion and the starburst at various scales. In this study, we investigated the relationship between the nuclear/circumnuclear starburst and AGN activity by considering both nuclear and the circumnuclear starbursts.

To investigate nuclear/circumnuclear starbursts, we used the polycyclic aromatic hydrocarbon (PAH) emission feature at $3.3 \mu\text{m}$, $6.2 \mu\text{m}$, $7.7 \mu\text{m}$, and $11.3 \mu\text{m}$. The PAHs are excited by far-UV photons and strong PAH emission are seen in star-forming regions, whereas a pure AGN shows only a featureless spectrum with virtually no PAH emission. Also, since the dust extinction is much lower for these $3.3 - 11.3 \mu\text{m}$ PAH emission ($\lesssim 0.06A_V$; Rieke & Lebofsky 1985; Lutz et al. 1996), we can quantitatively estimate modestly obscured

($A_V < 15$ mag) star-formation activity by using these emission lines. Throughout the paper, we adopted $H_0 = 80 \text{ kms}^{-1}\text{Mpc}^{-1}$, $\Omega_M = 0.3$, and $\Omega_\Lambda = 0.7$.

2. SAMPLE DATA

We studied 21 Seyfert 1 galaxies and 22 Seyfert 2 galaxies in the CfA (Huchra & Burg 1992) and $12 \mu\text{m}$ (Rush et al. 1993) samples selected based on their host-galaxy magnitudes and *IRAS* $12 \mu\text{m}$ fluxes, respectively. These samples are not expected to be biased toward or against the presence of nuclear starbursts. Our sample was selected from Imanishi & Wada (2004) data set with both the $3.3 \mu\text{m}$ PAH luminosity and the nuclear N-band luminosity. In their sample, Seyfert galaxies at $z = 0.008 - 0.035$ were selected to investigate the nuclear starburst by ground-based spectroscopy using a $1''\text{-}2''$ slit, where $1''$ corresponds to a physical scale of 150 ($z = 0.008$) to 650 pc ($z = 0.035$). Also, to be best observable from Mauna Kea, Hawaii, the declinations of Seyfert galaxies are limited to being larger than -30° . Owing to the telescope limit of the IRTF 3 m telescope, a restriction of declination of less than 68° is also applied. For their sample, there are no obvious biases.

Among 43 Seyfert galaxies, we estimated the supermassive black hole (SMBH) mass to investigate the mass accretion rate normalized with the AGN Eddington mass accretion rate for 25 objects. To these objects, we estimated the $6.2 \mu\text{m}$, $7.7 \mu\text{m}$, and $11.3 \mu\text{m}$ PAH emission for 13 objects further. Also, we collected the X-ray luminosity from the data in the literature for 15 objects. Since our sample included some upper limit data, we used statistical techniques applicable to a sample where upper limit data are present.

We focused on both nuclear starbursts, which exist within a few hundred parsecs from the center, and circumnuclear starbursts in the entire host galaxy region. Figure 1 shows the schematic view of the nuclear/circumnuclear starbursts. We can consider the $3.3 \mu\text{m}$ PAH emission, which were derived through ground-based spectroscopy using the narrow slit, as a nuclear starburst. Also, since a circumnuclear starburst is typically much higher than a nuclear starburst (see section 4.2), the $6.2 \mu\text{m}$, $7.7 \mu\text{m}$, and $11.3 \mu\text{m}$ PAH emission, which were observed in the whole host galaxy region, represent a circumnuclear starburst. In detail, we described in section 3.1 and 3.2.

3. ESTIMATION OF PHYSICAL PROPERTIES

3.1. Nuclear Starburst

PAH molecules near the AGN can be destroyed by strong X-ray radiation from the AGN (Voit 1992; Siebenmorgen et al. 2004). However, if the PAH molecules are sufficiently shielded by a substantial column density of X-ray-absorbing gas, PAHs can survive even if they exist near the AGN. In fact, ample gas is believed to exist that could be related to the obscuring material (the dusty torus in the context of the AGN unified model) around the AGN. In addition, the gravitational stability parameter \mathcal{Q} (Toomre 1964) decreases with the radius of the obscuring material, whose mass is notably smaller than that of the SMBH (Imanishi 2003). The gravitational collapse of molecular gas can therefore occur more easily in the outer part of the obscuring material. Thus, in the outer part of the obscuring material, a starburst could exist near the AGN and PAHs could survive. In fact, from the estimation of the surface brightness values of the $3.3 \mu\text{m}$ PAH emission (Imanishi & Alonso-Herrero 2004; Imanishi & Wada 2004), which were derived through ground-based spectroscopy using the $1''\text{-}2''$ slit, this emission should come from nuclear starbursts in the gas-rich region, which may be the obscuring material around AGN.

Therefore, we can use their $3.3 \mu\text{m}$ PAH emission data, which were observed by ground-based spectroscopy using the narrow slit, as the indicators of nuclear starbursts. Although the circumnuclear starburst, which often exhibit ring-like structures with a radius of kiloparsecs order from the center, along the slit direction could be also included, the fraction of the circumnuclear starburst emission inside this thin slit is negligible compared to the whole. Thus, the $3.3 \mu\text{m}$ PAH emission could be regarded as a practical probe for nuclear starbursts in both Seyfert 1 and Seyfert 2 galaxies.

In Imanishi (2003) and Imanishi & Wada (2004), only upper limits for the nuclear $3.3 \mu\text{m}$ PAH fluxes are available in more than half of the observed Seyfert galaxies. Additionally, the observed Seyfert galaxies do not comprise a complete sample. To increase the number and fraction of Seyfert galaxies with detectable nuclear $3.3 \mu\text{m}$ PAH emission, we newly observed eight sources, which are shown in Table 1. Among them, six sources (NGC 931, F03450+0055, NGC 262, NGC 513, MCG-3-58-7, and Mrk 993) showed possible signs of the $3.3 \mu\text{m}$ PAH emission in our previously obtained infrared $3\text{-}4 \mu\text{m}$ spectra (Imanishi 2003; Imanishi & Wada 2004). Therefore, we decided to re-observe these sources with longer exposure to check if the signs are real or not. The two sources (MCG-2-8-39 and 0152+06) are newly observed this time to increase the number of observed sources. We showed these observations in Appendix.

3.2. Circumnuclear Starburst

To estimate the absolute magnitudes of circumnuclear starburst activity in Seyfert galaxies, we analyzed archival infrared data obtained with the Infrared Spectrograph (IRS) (Houck et al. 2004) onboard the Spitzer Space Telescope (Werner et al. 2004) through the program PID 3269 (PI = Gallimore). We focused on the infrared spectra of Short-Low 2 (SL2; 5.2–7.7 μm) and 1 (SL1; 7.4–14.5 μm), to estimate the fluxes of PAH-emission features at $\lambda_{\text{rest}} = 6.2 \mu\text{m}$, 7.7 μm , and 11.3 μm in the rest frame.

We used the latest pipeline-processed data products at the time of our analysis (S11–14, pbcd files). The observations were performed with the slit-scan mode, and the entire host galaxy regions of the Seyfert galaxies were covered. We summed all the signals and extracted the spectra after subtracting the background emission in a standard manner. Thus, the resulting spectra should reflect the emission from the entire regions of the Seyfert galaxies. Wavelength and flux calibrations for the SL data were made on the basis of the files of the *Spitzer* pipeline-processed data, termed “b0_wavsamp.tbl” and “b0_fluxcon.tbl”, respectively. For SL1 spectra, data at $\lambda_{\text{obs}} > 14.5 \mu\text{m}$ in the observed frame are invalid (Infrared Spectrograph Data Handbook Version 1.0) and so were removed. For some faint sources, appropriate spectral binning was applied to reduce the scatter of data points and to achieve more reliable measurements of the PAH fluxes.

The circumnuclear starburst luminosity is typically much higher than the nuclear starburst luminosity (Imanishi 2003; Imanishi & Wada 2004, and see section 4.2). Thus, we can consider that the 6.2 μm , 7.7 μm , and 11.3 μm PAH emission, which were observed in the whole host galaxy regions, are good indicators of a circumnuclear starburst even if these PAH luminosity contain a small contribution from nuclear starbursts.

3.3. AGN Luminosity

For AGN activity, we used the nuclear N-band (10.5 μm) luminosity measured with a 1.5” aperture (Gorjian et al. 2004) since the contribution of starbursts for the nuclear N-band luminosity is small (Gorjian et al. 2004). However, nuclear N-band luminosity represents the reemission of hot dust illuminated by the AGN. So it may contain some uncertainties due to the dust distribution and the covering factor of the dusty torus around the AGN. To examine whether the nuclear N-band luminosity represents AGN activity in the sample data, we also used absorption-corrected hard (2–10 keV) X-ray luminosity, which is regarded as the AGN intrinsic luminosity for the Compton-thin AGN by using the data in the literature (see references in Table 3).

3.4. Black Hole Mass

Next, we estimated the SMBH mass, M_{BH} , to investigate the mass accretion rate normalized with the AGN Eddington mass accretion rate. To estimate SMBH masses of Seyfert 1 galaxies, we used the following method (in detail, see Kawakatu et al. 2007). The method for estimating the mass of a SMBH is based on the assumption that the motion of ionized gas clouds moving around the SMBH is dominated by the gravitational force and the clouds within the broad-line region (BLR) are virialized (e.g., Peterson & Wandel 1999). Adopting an empirical relationship (Kaspi et al. 2000) between the size of the BLR and the rest-frame optical continuum luminosity, $\lambda L_{\lambda}(5000\text{\AA})$ and reverberation mapping, we can obtain the following formula:

$$M_{\text{BH}} = 4.9_{-0.3}^{+0.4} \times 10^6 \left[\frac{\lambda L_{\lambda}(5100\text{\AA})}{10^{44} \text{ ergs s}^{-1}} \right]^{0.70 \pm 0.033} \left(\frac{v_{\text{FWHM}}}{10^3 \text{ km s}^{-1}} \right)^2 M_{\odot}. \quad (1)$$

We can use this equation for estimating the mass of SMBHs in Seyfert 1 galaxies.

We cannot use the above method for Seyfert 2 galaxies because no broad emission components exist. So we used the data of SMBH mass (Bian & Gu 2007), which is estimated by SMBH mass and the stellar velocity dispersion, σ_* , relation (Tremaine et al. 2002),

$$M_{\text{BH}} = 10^{8.13} \left(\frac{\sigma_*}{200 \text{ km s}^{-1}} \right)^{4.02} M_{\odot}. \quad (2)$$

4. RESULTS

4.1. Nuclear 3.3 μm PAH Emission

Figure 2 represents the zoom-in spectra around the 3.3 μm PAH emission feature of the observed Seyfert galaxies. Thanks to the excellent observing conditions and longer exposure, the flux excesses at the expected wavelength of the 3.3 μm PAH emission feature at $(1+z) \times 3.3 \mu\text{m}$ are now recognizable in the three sources (F03450+0055, NGC 513, and MCG-3-58-7), marked with “3.3 μm PAH” in Fig. 2. For these sources, the fluxes, luminosities, and rest-frame equivalent widths ($\text{EW}_{3.3\text{PAH}}$) of the 3.3 μm PAH emission were estimated using Gaussian fits. For the remaining five sources with no clear 3.3 μm PAH detection (marked with “3.3 μm PAH (?)” in Fig. 2), we estimated the upper limits of the PAH strengths, by adopting the lowest plausible continuum levels and assuming the profile of type-1 sources in Tokunaga et al. (1991) as a 3.3 μm PAH template. Table 2 summarizes the results.

At $\lambda_{\text{rest}} \sim 3.3 \mu\text{m}$ in the rest frame, Pf δ (3.30 μm) emission is present, superposed on

the 3.3 μm PAH emission. The relative contribution from this Pfd emission line is expected to be high in Seyfert 1 galaxies, because broad emission line components are unobscured. However, the equivalent width of the Pfd line is expected to be ~ 0.3 nm for a typical Seyfert 1 galaxy (Imanishi et al. 2006), and even lower in a Seyfert 2 galaxy. This equivalent width value is much lower than the observed values or upper limits in Table 2. We thus ascribe the flux excess at $\lambda_{\text{rest}} = 3.3$ μm mostly to the 3.3 μm PAH emission feature.

Among the six previously observed Seyfert galaxies, the detected 3.3 μm PAH fluxes or their upper limits are lower than previously derived upper limits (Imanishi 2003; Imanishi & Wada 2004), except NGC 931. For NGC 931, our new upper limit of the 3.3 μm PAH flux is $\sim 50\%$ higher than our previous estimate (Imanishi & Wada 2004), possibly because our new estimate is a conservative one, derived based on the lowest plausible continuum level. The 3–4 μm continuum flux levels are also similar within $\sim 50\%$ between the spectra in this paper and in our previous papers (Imanishi 2003; Imanishi & Wada 2004), except NGC 513. The flux of NGC 513 in this paper is more than 1 mag fainter than in Imanishi (2003), possibly because of narrower slit employed and/or the flux variation of the 3–4 μm continuum emission, originating in AGN-heated hot dust.

4.2. 6.2 μm , 7.7 μm , and 11.3 μm PAH Emission

Figure 3 and 4 represent 5.2–14.5 μm spectra of Seyfert 1 and 2 galaxies, respectively. Most of the Seyfert galaxies in Figure 3 and 4 show clearly detectable PAH emission features at $\lambda_{\text{rest}} = 6.2\mu\text{m}$, 7.7 μm , and 11.3 μm .

To estimate the fluxes of the PAH emission features at $\lambda_{\text{rest}} = 6.2$ μm , 7.7 μm , and 11.3 μm , we adopted a linear continuum determined from data points at the shorter and longer wavelength sides of individual PAH features, as used by Imanishi et al. (2007). The adopted continuum levels are shown as solid straight lines in Fig. 3 and 4. We fitted the PAH emission features with Gaussian profiles, which reproduced the observed data reasonably well. We treated the weak (lower than 3σ) or undetected PAH emission as the upper limit or non-flux, respectively.

By using 3.3 μm , 6.2 μm , and 11.3 μm PAH luminosities, we can roughly estimate infrared luminosities of the nuclear starburst and total starburst. In Table 4, we showed infrared luminosities of the nuclear starburst estimated from the 3.3 μm PAH luminosity; $L_{\text{IR},3.3} = L_{3.3} \times 10^3$ (Mouri et al. 1990; Imanishi 2002) and the total starburst estimated from the 6.2 μm and 11.3 μm PAH luminosity; $L_{\text{IR},6.2} = L_{6.2} \times 3 \times 10^2$ (Peeters et al. 2004) and $L_{\text{IR},11.3} = L_{11.3} \times 7 \times 10^2$ (Soifer et al. 2002), respectively. Infrared luminosities of the total

starbursts are several times or more as large as those of nuclear starbursts. This means that the circumnuclear starbursts dominate the total starburst luminosity. Thus, we can consider the $6.2 \mu\text{m}$, $7.7 \mu\text{m}$, and $11.3 \mu\text{m}$ PAH emission, which were observed in the whole host galaxy regions, as good indicators of a circumnuclear starburst.

4.3. Luminosity Correlation between Nuclear/Circumnuclear Starburst and AGN

In Figure 5, we checked a correlation between the nuclear N-band luminosity and the hard X-ray luminosity. We applied the generalized Kendall rank correlation statistics (Isobe et al. 1986) provided in the Astronomy Survival Analysis package (ASURV; Feigelson & Nelson 1985; Isobe et al. 1986) to both types of Seyfert galaxies. The probability that a correlation is not present was 0.9 % (2.6σ). Since these hard X-ray luminosity are the absorption-corrected luminosity and estimated for the Compton-thin AGN, this correlation means that the nuclear N-band luminosity is good indicator of AGN activity for these Seyfert galaxies samples.

In Figure 6, we plotted the nuclear N-band luminosity and the hard X-ray luminosity versus the $3.3 \mu\text{m}$ PAH emission luminosity. The probability that a correlation is not present was 0.7 % (2.7σ) and 5.3 % (1.9σ) for the nuclear N-band luminosity and the hard X-ray luminosity, respectively. Imanishi & Wada (2004) shows the positive correlation between the $3.3 \mu\text{m}$ luminosity and the nuclear N-band luminosity. We also obtained the same results for the hard X-ray luminosity. Thus, the correlation between the luminosity of the nuclear starbursts and central AGN is also statistically confirmed in Seyfert galaxies in hard X-ray luminosity, which is directly involved in AGN activity. These nuclear N-band and hard X-ray results definitely show that nuclear starburst luminosity is positively correlated with AGN power.

For hard X-ray luminosity - $3.3 \mu\text{m}$ PAH luminosity correlation, the correlation probability here is lower than that of the nuclear N-band luminosity. This difference may result from a large number of upper/lower limit data and few sample data. To analyze hard X-ray data in detail, we may need to eliminate these uncertainties and collect more data. We therefore focus on only the nuclear N-band luminosity for the following results.

In Figure 7, we plotted the nuclear N-band luminosity versus the energy for $6.2 \mu\text{m}$, $7.7 \mu\text{m}$, and $11.3 \mu\text{m}$ PAH emission. Here, we considered the $6.2 \mu\text{m}$, $7.7 \mu\text{m}$, and $11.3 \mu\text{m}$ PAH emission and plotted their energies. Since these PAH emission cover the whole host galaxy, we can consider them as indicators of circumnuclear starbursts. We also plotted the

energy for the $3.3 \mu\text{m}$ PAH emission in Fig. 7 and applied the generalized Kendall rank correlation statistics to these $6.2 \mu\text{m}$, $7.7 \mu\text{m}$, and $11.3 \mu\text{m}$ PAH emission simultaneously. The probability that a correlation is not present was found to be 0.35 % (2.9σ) for these PAH emission. Thus, not only nuclear starburst luminosity but also circumnuclear starburst luminosity are connected to AGN luminosity.

4.4. AGN Mass Accretion and Star-Forming Activity

In Figure 8, we also plotted the ratio of the nuclear N-band luminosity to the AGN Eddington luminosity, $L_{\text{N}1'.5}/L_{\text{Edd}}$ versus the energy of the nuclear/circumnuclear starbursts. The probability that a correlation is not present was found to be 4.8 % (2.0σ) for the nuclear starbursts ($3.3 \mu\text{m}$ PAH emission) and 16.7 % (1.4σ) for the circumnuclear starbursts (the other PAH emission). Thus, we statistically confirmed that the nuclear starburst is also positively correlated with the AGN luminosity normalized with the Eddington luminosity, whereas the circumnuclear starburst is only weakly correlated.

Here PAH emission are associated with star formation, and so the horizontal axis is also interpreted as an indicator of star-forming activity. The vertical axis also represents the mass accretion rate normalized with the Eddington mass accretion rate. This ratio corresponds to the efficiency of gas accretion onto a given SMBH mass. Thus, these results could be interpreted as the relationship between the efficiency of gas accretion onto a given SMBH mass and the star-forming activity around the AGN. Our results show a close correlation between the star-forming activity that is nearer the AGN and the efficiency of gas accretion. Therefore, starbursts near the AGN could affect AGN mass accretion more effectively.

5. Discussion: Link between AGN Mass Accretion and Nuclear/Circumnuclear Starbursts

We found that nuclear and circumnuclear starburst luminosities are positively correlated with AGN luminosity. However, nuclear starburst luminosity compared to circumnuclear luminosity is correlated with AGN mass accretion more strongly. These results imply that the AGN mass accretion could be connected the star formation activity around AGN. Therefore, here, we discuss the interpretation of our results focusing on the effect of star formation activities.

Umemura et al. (1997, 1998) showed the mass accretion onto the galactic center by the radiation effect from a circumnuclear starburst. They assumed a circumnuclear starburst

ring and a gas disk within starburst ring.

Through radial radiation pressure from the circumnuclear starburst, the optically thin surface layer of the gas disk (or the whole of the optically thin disk) is made to contract. Then the surface layer sheds angular momentum due to radiation drag. Also, since the radiation drag timescale for the dusty gas has been estimated a few 10^6 yr and the radial radiation pressure can influence at shorter timescale further (Umemura et al. 1998), due to these mechanisms, luminous starbursts could carry a larger amount of gas toward the inner region within the duration of the starburst phase; 10^7 yr (e.g., Efstathiou et al. 2000) and the typical age for AGNs; 10^8 yr (basically the Eddington timescale).

Radial radiation pressure may induce star formation as well as contraction of the gas disk shock (Umemura et al. 1998). The superbubble driven by sequential explosions of supernovae in an OB association located in the plane-stratified gas distribution may also compress the surrounding gas due to shock (Shapiro & Field 1976; Tomisaka & Ikeuchi 1986; Norman & Ikeuchi 1989) and new stars may be born there. In fact, Matsushita et al. (2005) showed the clear evidence of such a self-induced starburst at the inner edge of the expanding molecular superbubble in M82. This effect is even more expected in the case of a luminous starburst. If star formation is initiated in the contracted gas, it may induce further radiation effects and/or a superbubble in the inner gas disk. If the starbursts occur in such a sequential manner, the gas is carried farther into the inner region, and sequential starbursts may produce nuclear starbursts with some time lag (e.g., the timescale of the radiation pressure and radiation drag and/or the expansion time of the superbubble).

Also, Fukuda et al. (2000) showed that the gas ring in a barred galaxy could be unstable to gravitational instability and fragment into gas clumps. These clumps fall to the center by the torque from the massive clumps and/or by the dynamical friction from the stellar component (Makino 1997). Such dynamical effects could be also related to the gas accretion toward the center and produce nuclear starbursts.

Although the nuclear starburst is hidden by dusty gas, the structure is expected to be clumpy (Wada & Norman 2002). In this case, not only the chaotic disturbance of the gas but also the radiation drag from the nuclear starburst may be able to reduce the angular momentum of the clumpy gas (Kawakatu & Umemura 2002). Therefore, this innermost starburst could be directly related to the AGN mass accretion.

6. CONCLUSION

To determine whether the starbursts influence AGN activities, we investigated the correlation between nuclear/circumnuclear starbursts and AGN activities. We found that circumnuclear starburst luminosity as well as the nuclear starburst luminosity is positively correlated with AGN luminosity. Moreover, nuclear starburst is also positively correlated with the AGN luminosity normalized with the AGN Eddington luminosity, whereas the circumnuclear starburst is only weakly correlated. This implies that close connections exist between starbursts nearer the AGN and AGN mass accretion.

We thank K. Wada and T. Nagao for providing valuable discussions. We also thank the anonymous referee for valuable comments. Y.W. is supported by the Research Fellowship of the JSPS for Young Scientists. M.I. is supported by Grants-in-Aid for Scientific Research (19740109).

Appendix

The infrared 3–4 μm spectra of the eight Seyfert galaxies were taken using IRTF SpeX (Rayner et al. 2003). The 1.9–4.2 μm cross-dispersed mode with a $0''.8$ wide slit was employed. This mode enables L - (2.8–4.1 μm) and K -band (2–2.5 μm) spectra to be obtained simultaneously, with a spectral resolution of $R \sim 1000$. The sky conditions were photometric throughout the observations, and the seeing at K was measured to be in the range $0''.35$ – $0''.45$ FWHM. A standard telescope nodding technique (ABBA pattern) with a throw of $7''.5$ was employed along the slit. The telescope tracking was monitored with the infrared slit-viewer of SpeX. Each exposure was 15 sec, and 2 coadds were made at each position.

F- or G-type main sequence stars (Table 1) were observed as standard stars, with mean airmass difference of <0.1 to the individual Seyfert nuclei, to correct for the transmission of the Earth’s atmosphere and to provide flux calibration. The L -band magnitudes of the standard stars were estimated from their V -band ($\lambda = 0.6 \mu\text{m}$) magnitudes, adopting the $V - L$ colors appropriate to the stellar types of individual standard stars (Tokunaga 2000).

Standard data analysis procedures were employed, using IRAF¹. Initially, frames taken with an A (or B) beam were subtracted from frames subsequently taken with a B (or A)

¹ IRAF is distributed by the National Optical Astronomy Observatories, which are operated by the Association of Universities for Research in Astronomy, Inc. (AURA), under cooperative agreement with the National Science Foundation.

beam, and the resulting subtracted frames were added and divided by a spectroscopic flat image. Then, bad pixels and pixels hit by cosmic rays were replaced with the interpolated values of the surrounding pixels. Finally the spectra of Seyfert nuclei and standard stars were extracted, by integrating signals over $1''.8$ – $2''.2$, depending on actual signal profiles. Wavelength calibration was performed taking into account the wavelength-dependent transmission of the Earth's atmosphere. The spectra of Seyfert nuclei were divided by the observed spectra of standard stars, multiplied by the spectra of blackbodies with temperatures appropriate to individual standard stars (Table 1). Flux calibration was done based on signals of Seyfert galaxies and standard stars detected inside our slit spectra. To reduce the scatter of data points, appropriate spectral binning is employed, depending on the continuum flux levels of final spectra.

REFERENCES

- Barnes, J. E., & Hernquist, L. E. 1991, *ApJ*, 370, L65
- Barnes, J. E., & Hernquist, L. 1992, *ARA&A*, 30, 705
- Barth, A. J., Ho, L. C., Filippenko, A. V., & Sargent, W. L. 1995, *AJ*, 110, 1009
- Benedict, G. F., Smith, B. J., & Kenney, J. D. P. 1996, *AJ*, 112, 1318
- Bian, W., & Gu, Q. 2007, *ApJ*, 657, 159
- Buta, R., Purcell, G. B., & Crocker, D. A. 1995, *AJ*, 110, 1588
- Davies, R., Mueller Sanchez, F., Genzel, R., Tacconi, L., Hicks, E, Friedrich, S, & Sternberg, A. 2007, ArXiv e-prints, 704, arXiv:0704.1374
- Efstathiou, A., Rowan-Robinson, M., & Siebenmorgen, R. 2000, *MNRAS*, 313, 734
- Elmouttie, M., Koribalski, B., Gordon, S., Taylor, K., Houghton, S., Lavezzi, T., Haynes, R., & Jones, K. 1998, *MNRAS*, 297, 49
- Feigelson, E. D., & Nelson, P. I. 1985, *ApJ*, 293, 192
- Forbes, D. A., Norris, R. P., Williger, G. M., & Smith, R. C. 1994, *AJ*, 107, 984
- Fukuda, H., Habe, A., & Wada, K. 2000, *ApJ*, 529, 109
- Fukuda, H., Wada, K., & Habe, A. 1998, *MNRAS*, 295, 463

- Fukue, J., Umemura, M., & Mineshige, S. 1997, PASJ, 49, 673
- Gorjian, V., Werner, M. W., Jarrett, T. H., Cole, D. M., & Ressler, M. E. 2004, ApJ, 605, 156
- Hernquist, L. 1989, Nature, 340, 687
- Houck, J. R., et al. 2004, ApJS, 154, 18
- Huchra, J., & Burg, R. 1992, ApJ, 393, 90
- Imanishi, M. 2002, ApJ, 569, 44
- Imanishi, M. 2003, ApJ, 599, 918
- Imanishi, M., & Alonso-Herrero, A. 2004, ApJ, 614, 122
- Imanishi, M., Dudley, C. C., & Maloney, P. R. 2006, ApJ, 637, 114
- Imanishi, M., & Wada, K. 2004, ApJ, 617, 214
- Imanishi, M., Dudley, C. C., Maiolino, R., Maloney, P. R., Nakagawa, T., & Risaliti, G. 2007, ApJS, 171, 72
- Isobe, T., Feigelson, E. D., & Nelson, P. I. 1986, ApJ, 306, 490
- Kaspi, S., Smith, P. S., Netzer, H., Maoz, D., Jannuzi, B. T., & Giveon, U. 2000, ApJ, 533, 631
- Kawakatu, N., & Umemura, M. 2002, MNRAS, 329, 572
- Kawakatu, N., Imanishi, M., & Nagao, T. 2007, ApJ, 661, 660
- Knapen, J. H., Beckman, J. E., Heller, C. H., Shlosman, I., & de Jong, R. S. 1995, ApJ, 454, 623
- Knapen, J. H., Pérez-Ramírez, D., & Laine, S. 2002, MNRAS, 337, 808
- Knapen, J. H. 2005, A&A, 429, 141
- Leitherer, C., Vacca, W. D., Conti, P. S., Filippenko, A. V., Robert, C., & Sargent, W. L. W. 1996, ApJ, 465, 717
- Lutz, D., et al. 1996, A&A, 315, L269
- Maciejewski, W., Teuben, P. J., Sparke, L. S., & Stone, J. M. 2002, MNRAS, 329, 502

- Makino, J. 1997, *ApJ*, 478, 58
- Maoz, D., Barth, A. J., Sternberg, A., Filippenko, A. V., Ho, L. C., Macchetto, F. D., Rix, H.-W., & Schneider, D. P. 1996, *AJ*, 111, 2248
- Marconi, A., Moorwood, A. F. M., Origlia, L., & Oliva, E. 1994, *The Messenger*, 78, 20
- Matsushita, S., Kawabe, R., Kohno, K., Matsumoto, H., Tsuru, T. G., & Vila-Vilaró, B. 2005, *ApJ*, 618, 712
- Mauder, W., Weigelt, G., Appenzeller, I., & Wagner, S. J. 1994, *A&A*, 285, 44
- Mihos, J. C., & Hernquist, L. 1996, *ApJ*, 464, 641
- Montenegro, L. E., Yuan, C., & Elmegreen, B. G. 1999, *ApJ*, 520, 592
- Mouri, H., Kawara, K., Taniguchi, Y., & Nishida, M. 1990, *ApJ*, 356, L39
- Noguchi, M. 1988, *A&A*, 203, 259
- Norman, C. A., & Ikeuchi, S. 1989, *ApJ*, 345, 372
- Ohsuga, K., & Umemura, M. 1999, *ApJ*, 521, L13
- Ohsuga, K., Umemura, M., Fukue, J., & Mineshige, S. 1999, *PASJ*, 51, 345
- Ohsuga, K., & Umemura, M. 2001, *ApJ*, 559, 157
- O’Neill, P. M., Nandra, K., Papadakis, I. E., & Turner, T. J. 2005, *MNRAS*, 358, 1405
- Onodera, S., Koda, J., Sofue, Y., & Kohno, K. 2004, *PASJ*, 56, 439
- Panessa, F., & Bassani, L. 2002, *A&A*, 394, 435
- Panessa, F., Bassani, L., Cappi, M., Dadina, M., Barcons, X., Carrera, F. J., Ho, L. C., & Iwasawa, K. 2006, *A&A*, 455, 173
- Peeters, E., Spoon, H. W. W., & Tielens, A. G. G. M. 2004, *ApJ*, 613, 986
- Peterson, B. M., & Wandel, A. 1999, *ApJ*, 521, L95
- Pogge, R. W. 1989, *ApJ*, 345, 730
- Rayner, J. T., Toomey, D. W., Onaka, P. M., Denault, A. J., Stahlberger, W. E., Vacca, W. D., Cushing, M. C., & Wang, S. 2003, *PASP*, 115, 362

- Rieke, G. H., & Lebofsky, M. J. 1985, *ApJ*, 288, 618
- Rodríguez-Ardila, A., & Viegas, S. M. 2003, *MNRAS*, 340, L33
- Rush, B., Malkan, M. A., & Spinoglio, L. 1993, *ApJS*, 89, 1
- Saitoh, T. R., & Wada, K. 2004, *ApJ*, 615, L93
- Shapiro, P. R., & Field, G. B. 1976, *ApJ*, 205, 762
- Shinozaki, K., Miyaji, T., Ishisaki, Y., Ueda, Y., & Ogasaka, Y. 2006, *AJ*, 131, 2843
- Shlosman, I., Begelman, M. C., & Frank, J. 1990, *Nature*, 345, 679
- Siebenmorgen, R., Krügel, E., & Spoon, H. W. W. 2004, *A&A*, 414, 123
- Soifer, B. T., Neugebauer, G., Matthews, K., Egami, E., & Weinberger, A. J. 2002, *AJ*, 124, 2980
- Storchi-Bergmann, T., Wilson, A. S., & Baldwin, J. A. 1996, *ApJ*, 460, 252
- Taniguchi, Y. 1999, *ApJ*, 524, 65
- Thompson, T. A., Quataert, E., & Murray, N. 2005, *ApJ*, 630, 167
- Tokunaga, A. T. 2000, in *Allen's Astrophysical Quantities*, ed. A. N. Cox (4th ed; Berlin: Springer), 143
- Tokunaga A. T., Sellgren K., Smith R. G., Nagata T., Sakata A., Nakada Y., 1991, *ApJ*, 380, 452
- Tomisaka, K., & Ikeuchi, S. 1986, *PASJ*, 38, 697
- Toomre, A. 1964, *ApJ*, 139, 1217
- Tremaine, S., et al. 2002, *ApJ*, 574, 740
- Turner, T. J., George, I. M., Nandra, K., & Mushotzky, R. F. 1997, *ApJS*, 113, 23
- Umemura, M., Fukue, J., & Mineshige, S. 1997, *ApJ*, 479, L97
- Umemura, M., Fukue, J., & Mineshige, S. 1998, *MNRAS*, 299, 1123
- Voit, G. M. 1992, *MNRAS*, 258, 841
- Wada, K., Meurer, G., & Norman, C. A. 2002, *ApJ*, 577, 197

Wada, K., & Norman, C. A. 1999, ApJ, 516, L13

Wada, K., & Norman, C. A. 2001, ApJ, 547, 172

Wada, K., & Norman, C. A. 2002, ApJ, 566, L21

Watabe, Y., & Umemura, M. 2005, ApJ, 618, 649

Werner, M. W., et al. 2004, ApJS, 154, 1

Wilson, A. S., Helfer, T. T., Haniff, C. A., & Ward, M. J. 1991, ApJ, 381, 79

Table 1. Observing log

Object	Date	Telescope	Integration	P.A.	Name	Standard Stars		T_{eff} (K)	Remark
(1)	(UT)	Instrument	(Min)	($^{\circ}$)	(6)	L -mag	Type	(9)	(10)
NGC 931 (Mrk 1040)	2007 August 26	IRTF SpeX	96	0	HR 720	4.4	G0V	5930	$12\mu\text{m}$ Sy 1
F03450+0055	2007 August 28	IRTF SpeX	112	0	HR 962	3.7	F8V	6000	$12\mu\text{m}$ Sy 1
NGC 262	2007 August 31	IRTF SpeX	80	0	HR 410	5.0	F7V	6240	$12\mu\text{m}$ Sy 2
NGC 513	2007 August 27	IRTF SpeX	120	0	HR 410	5.0	F7V	6240	$12\mu\text{m}$ Sy 2
MCG-2-8-39	2007 August 30	IRTF SpeX	136	0	HR 784	4.5	F6V	6400	$12\mu\text{m}$ Sy 2
MCG-3-58-7	2007 August 30	IRTF SpeX	80	0	HR 8457	4.8	F6V	6400	$12\mu\text{m}$ Sy 2
Mrk 993	2007 August 31	IRTF SpeX	112	0	HR 410	5.0	F7V	6240	CfA Sy 2
0152+06 (UGC 1395)	2007 August 29	IRTF SpeX	120	0	HR 508	4.7	G3V	5800	CfA Sy 2

Note. — Column (1): Object. Col. (2): Observing date in UT. Col. (3): Telescope and instrument. Col. (4): Net on-source integration time in min. Col. (5): Position angle of the slit. 0° corresponds to the north-south direction. Col. (6): Standard star name. Col. (7): Adopted L -band magnitude. Col. (8): Stellar spectral type. Col. (9): Effective temperature. Col. (10): Seyfert 1 or 2 galaxy in the $12\mu\text{m}$ or CfA sample.

Table 2. Properties of the Nuclear 3.3 μm PAH Emission Feature

Object	$f_{\text{nuclear-3.3PAH}}$ ($\times 10^{-14}$ ergs s^{-1} cm^{-2})	$L_{\text{nuclear-3.3PAH}}$ ($\times 10^{40}$ ergs s^{-1})	rest $\text{EW}_{3.3\text{PAH}}$ (nm)
(1)	(2)	(3)	(4)
NGC 931	<6.5	<2.9	<2.5
F03450+0055	1.8	3.1	1.0
NGC 262	<3.3	<1.3	<1.6
NGC 513	0.5	0.3	3.5
MCG-2-8-39	<1.3	<2.0	<13
MCG-3-58-7	1.8	3.3	1.1
Mrk 993	<2.2	<0.9	<16
0152+06	<1.6	<0.8	<13

Note. — Column (1): Object. Col. (2): Observed nuclear 3.3 μm PAH flux. Col. (3): Observed nuclear 3.3 μm PAH luminosity. Col. (4): Rest frame equivalent width of the 3.3 μm PAH emission.

Table 3. Seyfert galaxies data

Object	z	$\log L_{3.3}$ (L_{\odot})	$\log L_{6.2}$ (L_{\odot})	$\log L_{7.7}$ (L_{\odot})	$\log L_{11.3}$ (L_{\odot})	$\log L_{N1^{0.5}}$ (L_{\odot})	$\log M_{\text{BH}}$ (M_{\odot})	$\log E_{\text{N}}$	$\log L_{\text{X}}$ (L_{\odot})	references
(1)	(2)	(3)	(4)	(5)	(6)	(7)	(8)	(9)	(10)	(11)
Seyfert 1 (CfA Sample)										
Mrk 335	0.025	6.85	?	?	?	10.06	6.89	-1.34	9.43	1
NGC 863 (Mrk 590)	0.027	<6.88	—	—	—	—	7.58	—	9.95	2
NGC 3786 (Mrk 744)	0.009	<6.36	—	—	—	—	7.53	—	—	—
NGC 4235	0.008	6.00	—	—	—	—	—	—	8.58	3
NGC 4253 (Mrk 766)	0.013	6.67	—	—	—	9.71	6.54	-1.34	9.09	1
NGC 5548	0.017	<6.76	—	—	—	10.01	7.92	-2.42	9.77	1
Mrk 817	0.031	7.36	8.41	8.7	8.2	10.43	7.72	-1.80	—	—
NGC 7469	0.016	<6.9	8.93	9.27	8.88	9.99	7.52	-2.04	9.61	1
Mrk 530 (NGC 7603)	0.029	7.24	8.56	8.64	8.48	10.01	—	—	—	—
Seyfert 1 (12 μm Sample)										
NGC 931 (Mrk 1040)	0.016	<6.88 [†]	<7.47	<8.22	7.87	9.82	7.13	-1.82	8.76	1
F03450+0055	0.031	6.91 [†]	?	?	?	10.07	—	—	—	—
3C 120	0.033	7.4	—	—	—	10.17	7.41	-1.76	10.38	2
Mrk 618	0.035	7.21	—	—	—	<9.95	—	—	—	—
MCG -5-13-17	0.013	<6.56	—	—	—	9.46	—	—	—	—
Mrk 79	0.022	<7.03	?	?	?	10.15	7.68	-2.05	—	—
Mrk 704	0.030	<6.95	—	—	—	10.52	—	—	—	—
NGC 2992	0.008	<6.44	—	—	—	9.10	—	—	9.30	2
Mrk 1239	0.019	<6.31	—	—	—	10.11	6.62	-1.02	—	—
MCG -2-33-34	0.014	6.53	—	—	—	<8.86	—	—	—	—
IC 4329A	0.016	<7.25	?	?	?	10.46	6.64	-0.69	9.95	1
Mrk 509	0.036	7.36	—	—	—	10.48	7.83	-1.86	—	—
Seyfert 2 (CfA Sample)										
NGC 4388	0.008	<6.03	7.68	8.17	7.73	9.24	7.22	-2.49	8.08	3
NGC 5252	0.023	<7.11	—	—	—	—	—	—	9.23	4
NGC 5256 (Mrk 266SW)	0.028	7.48	8.96	9.30	8.84	9.83	>6.92	< -1.60	—	—
NGC 5347	0.008	<6.26	<7.05	<7.45	<7.02	9.22	6.79	-2.08	—	—
NGC 5929	0.008	<5.59	<6.78	<7.32	<6.64	<8.37	7.25	< -3.39	—	—
NGC 7674	0.029	7.49	8.30	9.03	8.58	10.41	7.56	-1.66	—	—
Seyfert 2 (12 μm Sample)										
Mrk 938	0.019	7.82	—	—	—	9.85	—	—	—	—
NGC 262 (Mrk 348)	0.015	<6.53 [†]	<7.11	?	<7.29	9.52	7.21	-2.20	8.91	5
NGC 513	0.020	5.89 [†]	8.45	8.73	8.43	<9.69	7.65	< -2.47	—	—
NGC 1125	0.011	6.74	—	—	—	<8.95	—	—	—	—
NGC 1241	0.014	<5.97	<7.53	<7.63	<7.23	<9.38	7.46	< -2.59	—	—
NGC 1320 (Mrk 607)	0.010	6.44	—	—	—	9.45	7.18	-2.24	—	—
F04385-0820	0.015	6.61	—	—	—	9.64	—	—	—	—
NGC 1667	0.015	<6.21	8.7	9.05	8.65	<9.46	7.88	< -2.93	—	—
NGC 3660	0.012	6.4	—	—	—	<9.29	—	—	—	—
NGC 4968	0.010	6.59	—	—	—	9.49	—	—	—	—
MCG -3-34-64	0.017	<6.61	—	—	—	10.32	—	—	—	—
NGC 5135	0.014	7.12	—	—	—	9.46	7.35	-2.40	—	—
MCG -2-40-4 (NGC 5995)	0.024	<7.26	—	—	—	10.19	—	—	9.88	5
F15480-0344	0.030	<7.13	—	—	—	10.04	—	—	—	—
NGC 7172	0.009	<6.28	—	—	—	9.04	7.67	-3.14	9.29	2
MCG -3-58-7	0.032	<7.25	—	—	—	10.40	—	—	—	—

Note. — Column (1): Object. Col. (2): Redshift. Col. (3): PAH luminosity at 3.3 μm . [†] Taken from this paper. Col. (7): $L_{6.2}$, $L_{7.7}$, $L_{11.3}$, and $L_{N1^{0.5}}$ are the PAH luminosity at 6.2 μm , 7.7 μm , 11.2 μm , and the nuclear N-band (10.5 μm), respectively. Col. (8): Black hole mass. Col. (9): Ratio of nuclear N-band luminosity to AGN Eddington luminosity. Col. (10) and (11): Absorption-corrected hard (2-10 keV) X-ray luminosity and corresponding references; 1, O'Neill et al. (2005); 2, Shinozaki et al. (2006); 3, Panessa et al. (2006); 4, Turner et al. (1997); 5, Panessa & Bassani (2002). "—" shows no information. "?" means undetected PAH emission.

Table 4. Infrared luminosity

Object	$\log L_{\text{IR},3.3}$ (L_{\odot})	$\log L_{\text{IR},6.2}$ (L_{\odot})	$\log L_{\text{IR},11.3}$ (L_{\odot})	$L_{\text{IR},6.2}/L_{\text{IR},3.3}$	$L_{\text{IR},11.3}/L_{\text{IR},3.3}$
(1)	(2)	(3)	(4)	(5)	(6)
Mrk 817	10.36	10.88	11.05	3.30	4.94
NGC 7469	< 9.90	11.40	11.73	> 31.52	> 68.21
Mrk 530 (NGC 7603)	10.24	11.03	11.33	6.14	12.41
NGC 931 (Mrk 1040)	< 9.88	< 9.94	10.72	—	> 6.98
NGC 4388	< 9.03	10.15	10.58	> 13.14	> 35.80
NGC 5256 (Mrk 266SW)	10.48	11.43	11.69	8.88	16.36
NGC 5347	< 9.26	< 9.52	< 9.87	—	—
NGC 5929	< 8.59	< 9.25	< 9.49	—	—
NGC 7674	10.49	10.77	11.43	1.90	8.79
NGC 262 (Mrk 348)	< 9.53	< 9.58	< 10.14	—	—
NGC 513	8.89	10.92	11.28	106.79	247.67
NGC 1241	< 8.97	< 10.00	< 10.08	—	—
NGC 1667	< 9.21	11.17	11.50	> 90.89	> 196.73

Note. — Column (1): Object. Column (2): Infrared luminosity of the nuclear starburst. $L_{\text{IR},3.3} = L_{3.3} \times 10^3$ (Mouri et al. 1990; Imanishi 2002). Col. (3) and (4): $L_{\text{IR},6.2} = L_{6.2} \times 3 \times 10^2$ (Peeters et al. 2004) and $L_{\text{IR},11.3} = L_{11.3} \times 7 \times 10^2$ (Soifer et al. 2002) are the infrared luminosity of total starbursts, which were estimated from 6.2 μm and 11.3 μm PAH luminosity, respectively. Col. (5) and (6): Infrared luminosity Ratios of total starburst to nuclear starburst. "—" shows that both the infrared luminosity of the nuclear starburst and the total starburst are upper limit data.

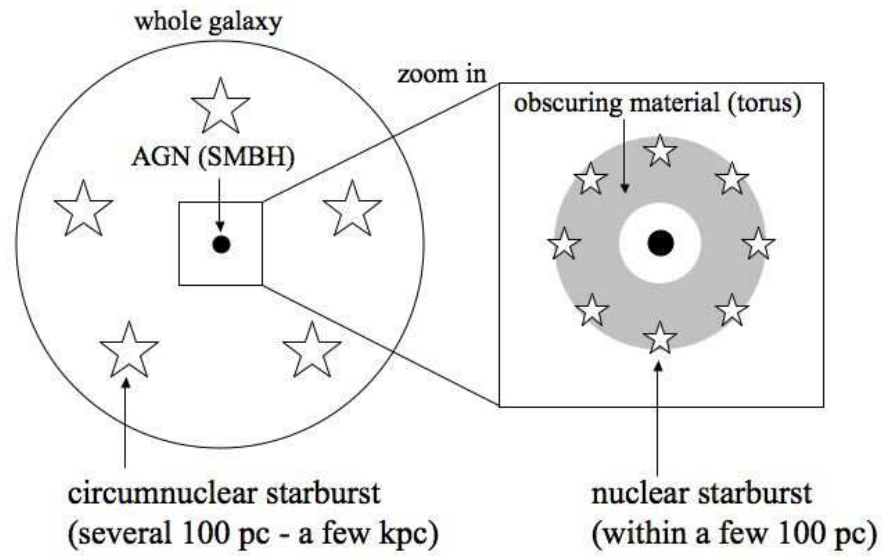


Fig. 1.— The schematic view of the nuclear/circumnuclear starbursts. The nuclear starburst (within a few 100 pc) and the circumnuclear starburst (several 100 pc - a few kpc) are distributed around AGN.

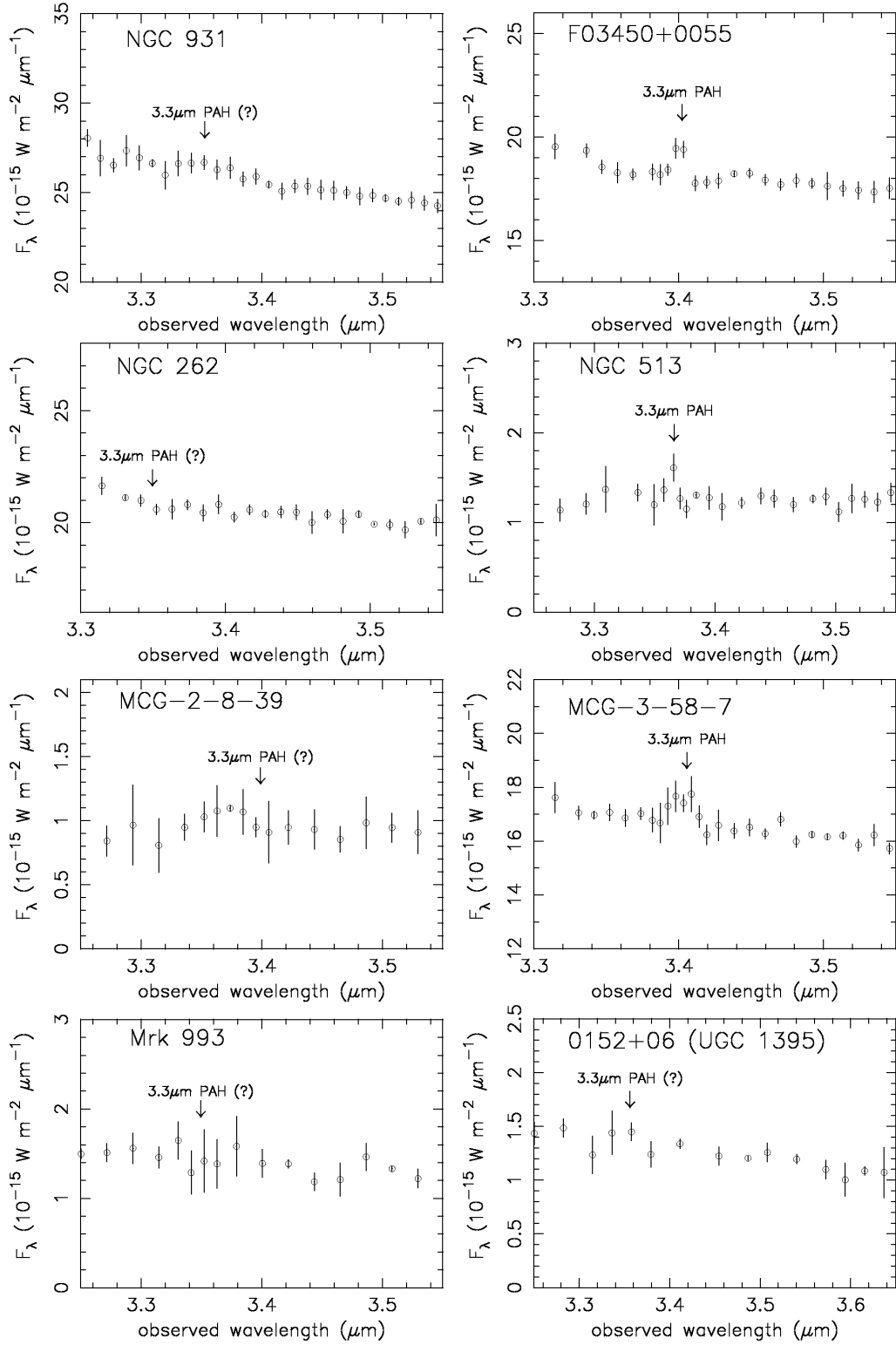


Fig. 2.— Zoom-in spectra around the redshifted $3.3 \mu\text{m}$ PAH emission feature (lower arrows) of the observed eight Seyfert galaxies. The horizontal and vertical axes are the observed wavelength in μm and F_λ in $10^{-15} \text{ W m}^{-2} \mu\text{m}^{-1}$, respectively.

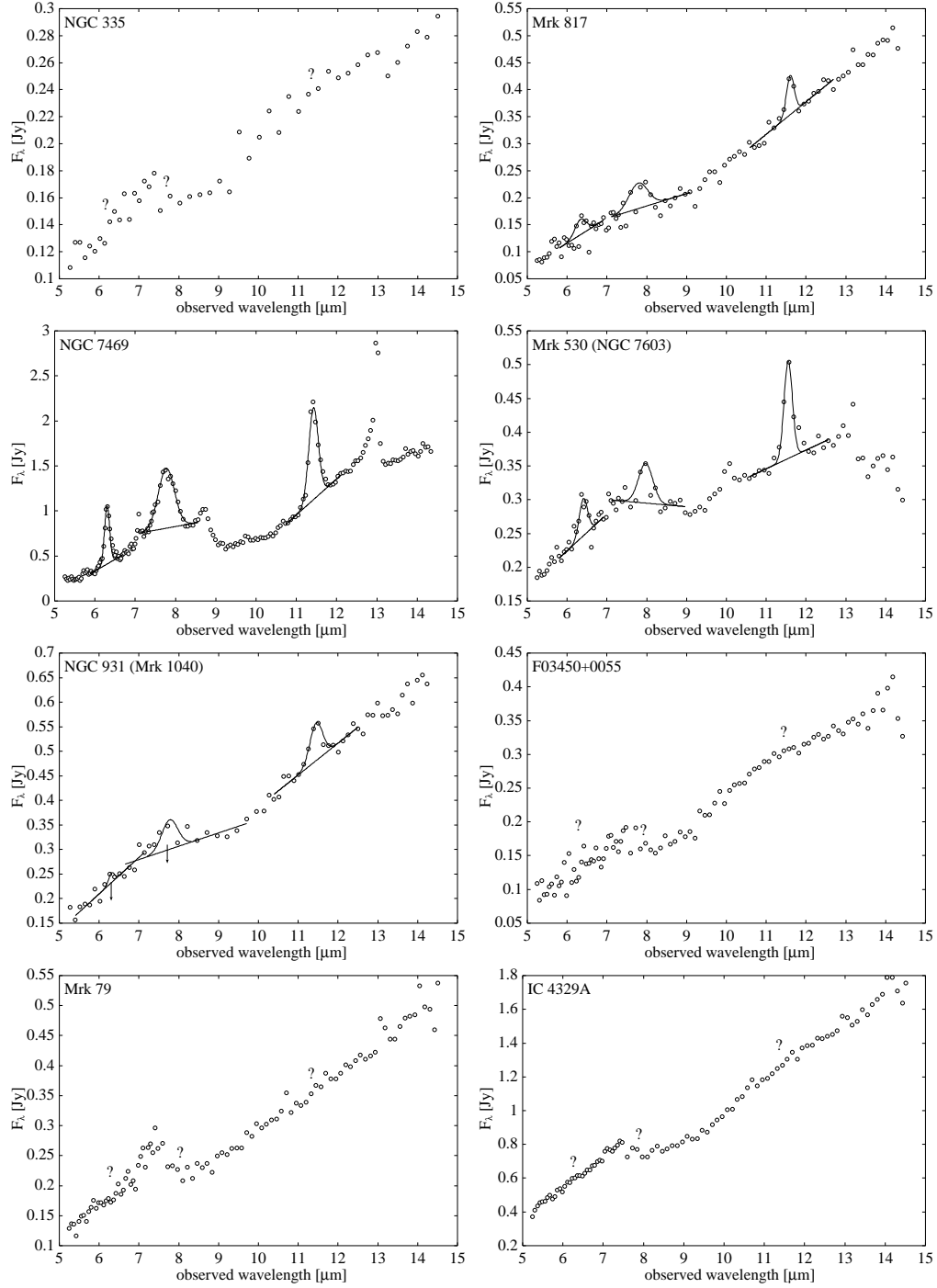


Fig. 3.— 5.2 – 14.5 μ m spectra of Seyfert 1 galaxies. The horizontal and vertical axes are the observed wavelength in μ m and F_{λ} in Jy, respectively. The solid straight lines are the adopted continuum to estimate each PAH emission fluxes. The solid curves are Gaussian profile fittings of PAH emission. The lower arrows and the question marks indicate the weak (lower than 3σ) and undetected PAH emission, respectively.

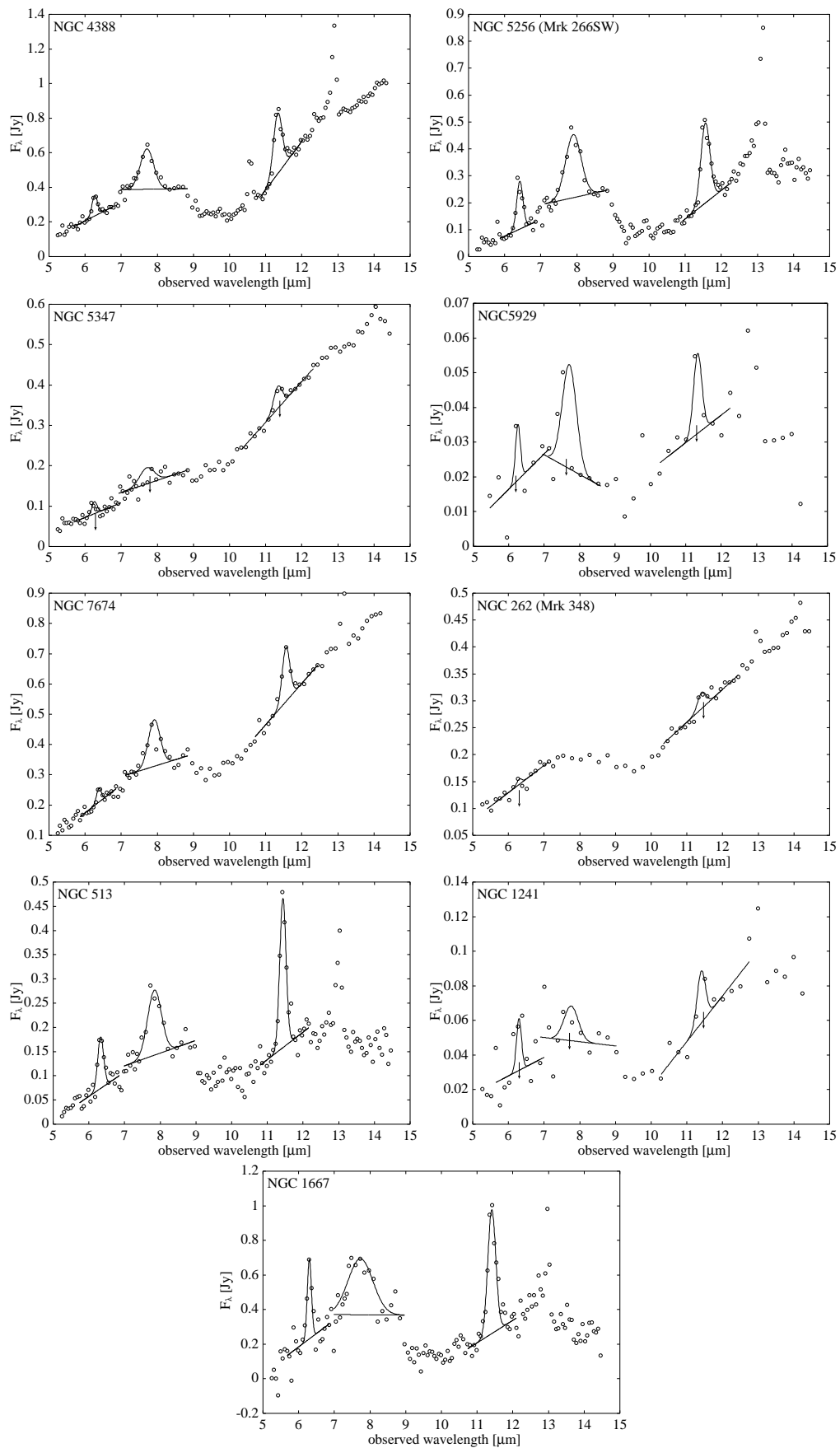


Fig. 4.— Same as Fig. 3, but these spectra are Seyfert 2 galaxies

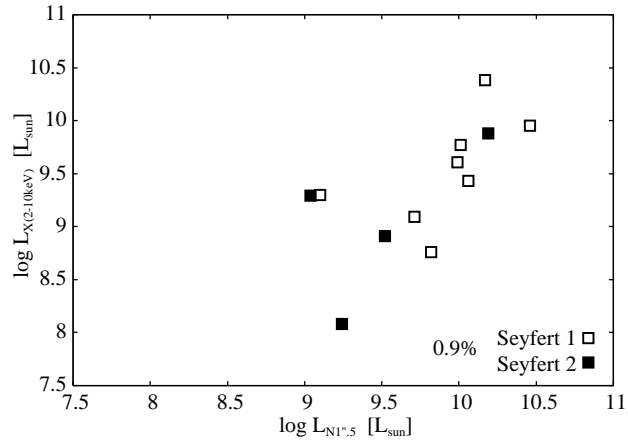


Fig. 5.— The horizontal and the vertical axes are the nuclear N-band luminosity and the absorption-corrected hard (2-10 keV) X-ray luminosity, respectively. The percentage represents the probability that a correlation is not present.

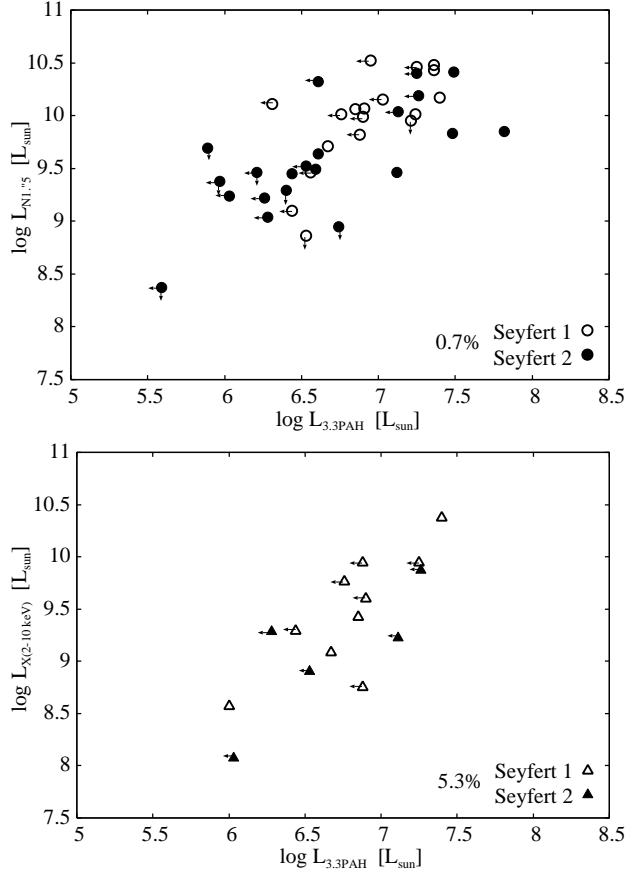


Fig. 6.— *upper*: The horizontal axis is nuclear $3.3 \mu\text{m}$ PAH emission luminosity detected inside slit spectra (Imanishi & Wada (2004) and this paper). The vertical axis represents the nuclear N-band ($10.5 \mu\text{m}$) luminosity measured with ground-based two-dimensional camera with a $1''.5$ aperture (Gorjian et al. 2004). *bottom*: Same as upper figure, but the vertical axis represents the absorption-corrected hard (2-10 keV) X-ray luminosity. The percentage represents the probability that a correlation is not present.

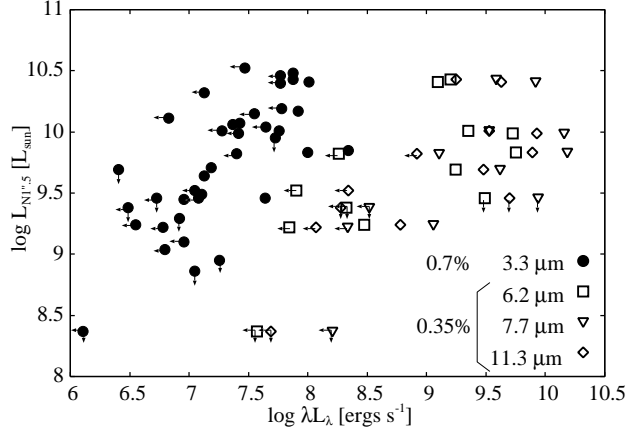


Fig. 7.— The horizontal axis is the energy of the 3.3 μm , 6.2 μm , 7.7 μm , and 11.3 μm PAH emission and the vertical axis is the nuclear N-band luminosity. The percentages represent the probability that a correlation is not present.

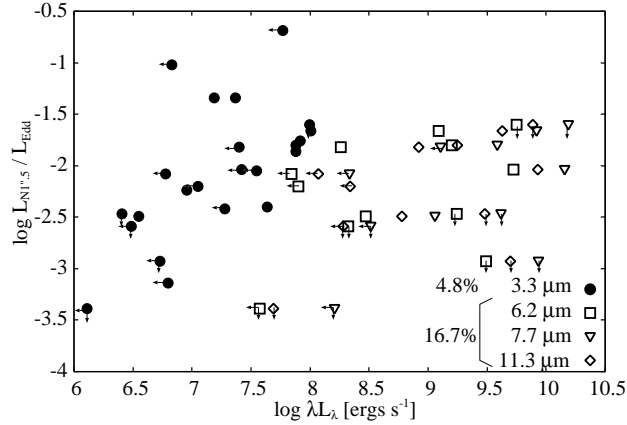


Fig. 8.— Same as Fig. 7, but the vertical axis represents the ratio of the nuclear N-band luminosity to the AGN Eddington luminosity.